Efficient calculation of α- and β-nitrogen free energies and coexistence conditions via overlap sampling with targeted perturbation

Tai Boon Tan, Andrew J. Schultz, and David A. Kofke[a)]
Department of Chemical and Biological Engineering, University at Buffalo, The State University of New York, Buffalo, New York 14260-4200, USA

(Received 29 April 2011; accepted 7 July 2011; published online 29 July 2011)

A recently introduced solid-phase free-energy calculation method that is based upon overlap sampling with targeted free-energy perturbation is further developed and extended to systems with orientational degrees of freedom. Specifically we calculate the absolute free energy of the linear-molecular nitrogen model of Etter *et al*., examining both the low-temperature low-pressure α-N_2 structure and the orientationally disordered β-N_2 phase. In each perturbation (for the α-N_2 phase) to determine the free-energy difference between systems at adjacent temperatures, harmonic coordinate scaling is applied to both the translational and rotational degrees of freedom in the nitrogen molecule to increase the phase-space overlap of the two perturbing systems and consequently, improve the free-energy difference results. For the plastic β-N_2 phase, a novel method that requires several perturbation paths is introduced to calculate its absolute free energy. Through these methods, the absolute free energies for both the α-N_2 and β-N_2 phase can be accurately and precisely determined. We find again that the anharmonic contribution to the free energy has weak dependence on system size. The transition properties for the α-N_2 and β-N_2 phase are also investigated. The α-β phase transition for the model at atmospheric pressure (0.1 MPa) is found to occur at 40.35 ± 0.01 K with volumetric and entropy changes of 0.44 ± 0.01 cm^3/mol and 1.99 ± 0.01 cal/mol.K respectively. © *2011 American Institute of Physics*. [doi:10.1063/1.3615941]

I. BACKGROUND AND INTRODUCTION

Great interest and effort have been devoted by researchers to understand and predict the occurrence of crystal polymorphism. Contamination by undesirable polymorphs during manufacturing and production has been an issue of considerable concern in the pharmaceutical industry in particular. Examination of the free energy is crucial in understanding the stability of crystals and in locating thermodynamic phase equilibria. The process of crystallization is affected by many factors, and not all of them thermodynamic, so free energy is not the only consideration in designing a crystallization process. Nevertheless it is certainly helpful to know the relative free energies of any candidate polymorphs when considering which ones might emerge. This is true even if the most stable one is not the one produced by a process, if only to raise awareness of how a process could go wrong. Absent other considerations, the most probable molecular crystal tends to occupy the lowest free energy, so the ability to characterize possible polymorphs will still rely mainly on the stability as dictated by their thermodynamics. However, at present our ability to predict the free energy of a particular molecular crystal, and thus to rank the stability of different crystal structures, still has much room for improvement.

Polymorphism has impacted primarily the pharmaceutical industry in various aspects. Different crystalline forms of the same drug substance often exhibit different physical properties. One of the most important properties is the solubility of the drug, which can differ for a substance in different polymorphic forms owing to the differing free energies of the respective polymorphs. The variation in solubility of different polymorphs in the human body directly affects its bioavailability and its efficacy. It can be a major problem if the polymorphs of the active pharmaceutical ingredients are not well understood and identified. A well-known and costly example[1] is the unexpected emergence of a second crystalline form during manufacture of Ritonavir, a protease inhibitor for human immunodeficiency virus. The new form was found to be thermodynamically more stable and less soluble than the one that was initially synthesized.

Although the free energy is the key to gauging relative stability of competing or plausible polymorphs, most polymorph screening and identification routines consider only the enthalpic contribution to the crystal stability. Some of these procedures are elegantly implemented and have shown success in prediction in the recent Crystal Structure Prediction Contest (CSP) (Ref. 2) organized by the Cambridge Crystallography Center. The enthalpy is only an approximation to the free energy, and accordingly it is likely that the predictions can be improved by including the entropic contribution, perhaps following an initial enthalpy-based screen to identify the most likely candidate polymorphs. The importance of the entropy to the solid-solid phase transition has been highlighted through the work published by Gavezotti and Fillipini.[3]

Methods for comparing stability of crystal structures must work with molecular-scale models, to which molecular simulation methods are applied to evaluate or estimate the free energy. Many such methods exist.[4] Among those that aim to yield the true free energy (rather than an estimate, such as

[a)]Author to whom correspondence should be addressed. Electronic mail: kofke@buffalo.edu.

is given by the lattice energy alone), the most commonly used technique is that due to Frenkel and Ladd.[5] In this method, thermodynamic integration is employed to traverse a path from the Einstein crystal to solid of interest, to evaluate the free energy difference between the target and model systems. The method is somewhat computationally intensive, and this is a significant consideration if being applied for polymorph screening purposes, where the free energy of numerous structures may be of interest. In such a context it is worthwhile to consider whether more efficient but equally accurate approaches can be developed and applied.

Many crystalline solids can be approximated as a lattice of interacting harmonic oscillators, with behavior that is analytically tractable. Recently, we proposed[6] harmonically targeted temperature perturbation (HTTP) as a method that exploits the approximate harmonic character of crystals to yield accurate values of the free energy with great efficiency. In fact the output of the HTTP calculation is specifically the difference in free energy between the actual system and its harmonic approximation. This feature lends two advantages in particular. First, this difference may be small compared to the full free energy, so the stochastic error involved in its calculation will be proportionately small as well (in other words, were the method applied to a system that is truly harmonic, it would provide a result having no stochastic error at all). Second, it appears that finite-size effects may be largely captured by the harmonic component of the free energy, so relatively small system sizes may be used when computing the free energy using the HTTP method.

We demonstrated the HTTP method through application to soft-sphere (inverse-power) models with various degrees of softness.[6] We obtained results with high precision, and among other things we confirmed the relative stabilities of different crystal structures and demonstrated that entropic contributions were quite significant in comparison to the free-energy differences between candidate structures. In the present work we extend the HTTP method in the context of polymorphism through application to a non-spherical molecule – *viz*. the linear nitrogen model. We show how extension of the HTTP method is accomplished in this case (and implicitly for other more complicated molecules), and we examine for this system the importance of entropic contributions as well as the nature of finite-size effects.

The solid phases of nitrogen have been investigated both through experiments[7] and molecular simulation[8–10] due to its very interesting diverse phases. The phase diagram of solid nitrogen was introduced by Mills *et al*.,[11] showing that solid nitrogen exists in at least six different structures over a wide range of pressures and temperatures, with each phase exhibiting distinct properties. All the low-temperature structures occupy orientationally ordered phases, where the molecular axis of each molecule has a nominal orientation in the unit cell. On the other hand, the high-temperature structures, the β- and δ-phase in particular, appear in orientationally disordered plastic phases.

In this study, we examine the solid-solid phase transition between the α- and β-phase by calculating their absolute free energies using the molecular model proposed by Etter *et al*.[12] The first-order phase transition between the α- and β-phase was determined experimentally through x-ray and calorimetric studies[7] to occur at 35.6 K and ambient pressure (0.1 MPa). The low-temperature α-phase structure has been well studied and characterized. The α-phase solid nitrogen occupies an fcc-crystal packing with four molecules in a cubic unit cell and the molecules orient along the body diagonals with symmetry of Pa3. The molecules for the high-temperature orientationally disordered β-phase are packed on a hexagonal lattice (hcp) of $P6_3/mmc$ space group. The layers of molecules are stacked in an ABABAB… sequence with an almost ideal c/a ratio.

The presentation of this paper is arranged such that we first review in Sec. II the formalism and the methods that we employ in this study. Section III presents and discusses our results, and we end with concluding remarks for our findings in this work in Sec. IV.

II. FORMALISM AND METHOD

In this section, we demonstrate the procedures and methods to obtain the absolute free energies for both the orientationally ordered (α-N_2) and disordered (β-N_2) phases. Before we start, let us briefly review the solid-phase free-energy technique that has already been detailed in previous work.[6] The HTTP method provides a means for efficiently computing the difference in free energy for a system at two different temperatures. The approach is an implementation of the general targeted free-energy perturbation (FEP) method suggested by Jarzynski,[13] although modified to use overlap sampling rather than direct perturbation. As such, perturbation in the temperature is accompanied by perturbation in the atom positions, applying the harmonic approximation to target the displacements. All atom positions are scaled away from (if perturbing to higher temperature) or toward (if perturbing to lower temperature) their respective lattice sites in proportion to the square root of the temperature ratios. For a perfectly harmonic system, this means that the ratio of energy to temperature, U/T would be unchanged, and the perturbation average would indicate a zero free energy difference; when the harmonic component is added to this result (which emerges as a Jacobian for the coordinate transformation), the exact free energy is obtained. Thus the quantity measured by the method is strictly the change in the anharmonic contribution βA_C to the free energy. Changes for large differences in temperature are computed by summing results for smaller temperature perturbations, and overlap sampling[14] (Bennett's method) (Ref. 15) is applied to span each temperature interval to promote accuracy and efficiency in the calculations.

In the context of using the HTTP method, one can compute the absolute, classical free energy of a target system by computing the free-energy difference down to very low temperature T_ε, where the harmonic approximation becomes highly accurate. The small low-temperature anharmonic correction can be evaluated by a harmonic perturbation,[6] or by executing an extrapolation scheme as has been described by Tan *et al*.[6] Complication can arise if the system is not thermodynamically stable at low temperature, in which case constraints can be introduced to stabilize the system and enable calculation of a low-temperature reference free energy.

The harmonic free energy can be obtained through the diagonalization of the $mN \times mN$ Hessian matrix, where m and N are the degrees of freedom (dof) per particle and number of particles in the system, respectively. The equation of the harmonic free energy of a system can be expressed[6,16] as

$$\frac{\beta A_{\text{harm}}}{N} = \frac{\beta U_{\text{lat}}}{N} + \frac{1}{2N}\sum_{i}^{mN-3} \ln\left(\frac{\lambda_i}{2\pi kT}\right) - \frac{3}{2}\frac{\ln N}{N} + \frac{1}{N}\ln\rho, \tag{1}$$

where λ_i are the eigenvalues determined from decomposing the Hessian matrix and U_{lat} is the lattice energy, ρ is the molecular density, k is the Boltzmann constant, and T is the absolute temperature. The last two terms on the RHS of the equation are contributions from center-of-mass motion and vanish in the thermodynamic limit $N \to \infty$.

In this method, the general working equation to obtain the absolute solid-phase free energy of a system is simply expressed as:

$$\frac{\beta A}{N} = \frac{\beta A_{\text{harm}}}{N} + \frac{\beta A_C}{N}. \tag{2}$$

In what that follows, we present the methods that we employ to calculate the anharmonic term, βA_C appearing in Eq. (2), for the orientationally ordered (α-N_2) and disordered (β-N_2) phase. For the α-N_2 phase, the calculation is similar to what was developed in our previous work, but with harmonic-scaling applied not only to the molecular displacement but also to its orientation. For the orientationally disordered β-N_2 free-energy calculation, we must introduce an additional perturbation path that allows a gradual transition for the system to a "free rotor" or orientationally disordered structure. With this, we introduce a novel method – rotational targeted perturbation (RTP), combined with the HTTP method to calculate the free energy for an orientationally disordered phase. Both the HTTP and RTP methods are formulated using a two-stage FEP implementation, specifically the Bennett-optimized overlap sampling technique.[15] This sampling technique has been outlined in Refs. 6 and 17 and we will provide only a brief review of the main equation that is relevant for the application here. The primary focus will be given to the development of the absolute free-energy calculation for the orientationally disordered phase. We first illustrate the rotational coordinates that we employ in this study and then follow by the full demonstration of free-energy calculations for both the α-N_2 and β-N_2 phases.

A. Rotational coordinates

The strategy in general for targeted perturbation is to couple the perturbation of interest in the Hamilton with a deformation of the molecular coordinates, so that after the perturbation the system is in a configuration that is more likely to be appropriate to the perturbed Hamiltonian. Application of this idea to rotational coordinates is a bit less straightforward than for the simple Cartesian translational coordinates encountered in previous applications. We begin by defining our coordinate system that describes the orientation of a rigid linear molecule in the context of targeted perturbations of the orientation.

Each molecule in a given phase has associated with it a nominal orientation, $\hat{a}_0$, which in the present application is the molecule's orientation for the minimum-energy configuration consistent with the lattice symmetry of the phase. The usual axial and azimuthal angles θ and ϕ can be defined with respect to this axis, but these are not always convenient coordinates for the present application. Instead we introduce alternative coordinates (κ_1, κ_2) defined in terms of the projection of the molecule's orientation $\hat{R}$ onto the plane perpendicular to $\hat{a}_0$, defined by the axes $\hat{a}_1$ and $\hat{a}_2$ such that $\hat{a}_0$, $\hat{a}_1$, and $\hat{a}_2$ form an orthonormal basis for a three-dimensional Euclidean space; see Fig. 1(a). In particular,

$$\kappa_1 = \kappa(\hat{R}\cdot\hat{a}_1), \tag{3a}$$

$$\kappa_2 = \kappa(\hat{R}\cdot\hat{a}_2), \tag{3b}$$

where

$$\kappa = \frac{\sqrt{2(1-\cos\theta)}}{\sin\theta} = \frac{2\sin(\theta/2)}{\sin\theta}. \tag{3c}$$

With this definition, the points (κ_1, κ_2) lie on a circle with area $2\pi(1-\cos\theta)$, equal to the area of a spherical cap swept out around $\hat{a}_0$ by a vector at angle θ; see Fig. 1(b). Consequently

$$d\kappa_1 d\kappa_2 = \sin\theta d\theta d\phi.$$

Thus the Jacobian for a transformation that scales each $\boldsymbol{\kappa}_i$ coordinate by a common factor λ is simply λ^2. The $\boldsymbol{\kappa}_i$ coordinates are also desirable in the present context because they are better suited than θ and ϕ for forming the Hessian matrix needed to conduct the harmonic analysis.

B. Free-energy calculation for orientationally ordered α-N_2 phase

The procedure to calculate the anharmonic term, βA_C, for the α-N_2 phase follows the HTTP method.[6] However, instead of applying the harmonic scaling to only the translational coordinates during the perturbation calculation, we apply it to the rotational coordinates as well. Thus scaling is performed on a total of five degrees of freedom per molecule – the three molecular deviations from the respective lattice sites, and the two orientational coordinates $\boldsymbol{\kappa}_1$ and $\boldsymbol{\kappa}_2$. Specifically, when perturbing from temperature T_I to T_{II}, the Cartesian displacement of each molecule's center of mass (COM) relative to its nominal lattice position, $\mathbf{r}_i - \mathbf{r}_{i,\text{lat}}$, is scaled by $(T_{II}/T_I)^{1/2}$, so the COM coordinates transform as

$$\mathbf{r}_{i,II} = \mathbf{r}_{i,\text{lat}} + \left(\frac{T_{II}}{T_I}\right)^{1/2}(\mathbf{r}_{i,I} - \mathbf{r}_{i,\text{lat}}). \tag{4}$$

Likewise, the orientation coordinates transform according to the equation given below:

$$\boldsymbol{\kappa}_{i,II} = \left(\frac{T_{II}}{T_I}\right)^{1/2}\boldsymbol{\kappa}_{i,I}. \tag{5}$$

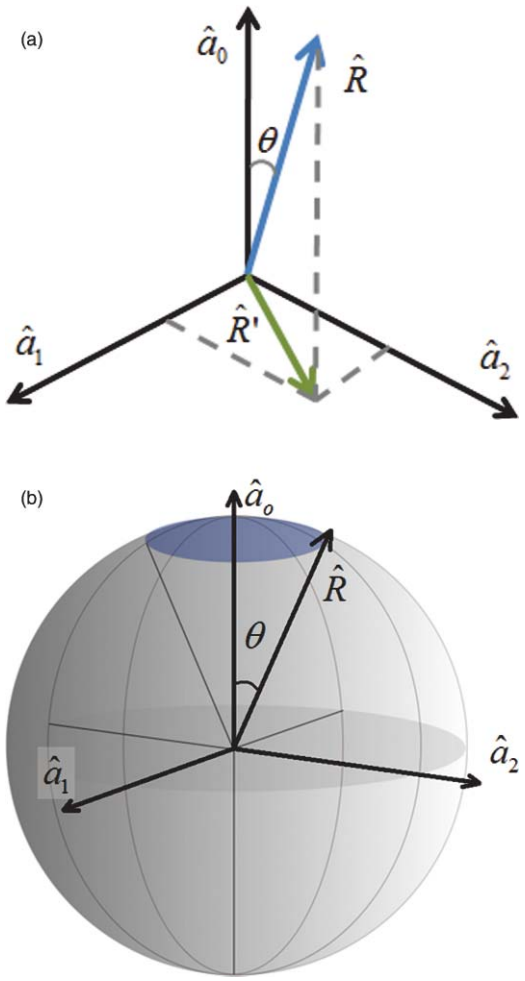

FIG. 1. (a) Coordinate definition for linear-molecule orientation. $\hat{R}$ is the molecular orientation vector, which rotates an angle θ off its nominal orientation $\hat{a}_0$. $\hat{a}_0$, $\hat{a}_1$, and $\hat{a}_2$ are mutually orthogonal. $\hat{R}'$ represents the projection of vector $\hat{R}$ on the plane that is perpendicular to $\hat{a}_0$. (b) Graphical illustration of the relationship between the rotation angle and the spherical surface area. $\hat{a}_0$ is the nominal molecular orientation. The shaded blue spherical cap represents the surface area, $2\pi(1-\cos\theta)$, around $\hat{a}_0$ within the angle θ.

The overlap sampling technique is employed to evaluate free energy differences. The overlap weight function is defined as

$$\gamma = \frac{e_I e_{II}}{e_{II} + \alpha e_I}, \tag{6}$$

where e_i is the Boltzmann factor for system i, after application of any coordinate transformations used for targeted perturbation. The parameter α is the optimized Bennett's parameter, where the optimum value of α is given as $\alpha \approx \exp[-\Delta(\beta A_C)]$ and $\Delta(\beta A_C)$ is the free-energy difference between systems I and II, excluding any contributions captured by the Jacobian for the coordinate transformation (so for HTTP, this is the anharmonic contribution to the free energy). $\Delta(\beta A_C)$ is given self-consistently in terms of the perturbation averages

$$\exp[-\Delta\beta A_C] = \langle \gamma / e_I \rangle_{e_I} / \langle \gamma / e_{II} \rangle_{e_{II}} \tag{7}$$

To obtain the absolute free energy, an extrapolation approach[6] is applied to connect the α-N_2 phase at low temperature to the harmonic system. For this purpose we fit $\Delta\beta A_C(T)$ to the form:

$$\beta A_C^{\text{fit}}(T) = \sum_{i=1}^{P} a_i T^i + \exp(-bT^d) \sum_{i=1}^{Q} c_i T^i. \tag{8}$$

By construction, the fitting function constrains βA_C to be zero at $T = 0$. P and Q define the order of the polynomials that appear in the function. b and d are fitting parameters, as are the a_i and c_i.

Although the α-N_2 phase is an orientationally ordered structure, at sufficiently high temperature the molecules will ultimately lose their orientation preference. To ensure the validity of the scaling of the two orientational coordinates, such that the scaled molecular orientation does not exceed 90° off the nominal orientation, a hard constraint is imposed at a 90° angle. Note that this hard constraint potential does not prevent the system from becoming disordered. For the purpose of suppressing the disorder of the α-N_2 system in orientational dof at high temperatures, we introduce a system constraint that imposes the condition: $\langle \cos\theta \rangle > 0.8$, where $\langle \cos\theta \rangle$ is the molecule-averaged cosine angle θ (as shown in Fig. 1(a)) of the system in a specific configuration.

C. Free-energy calculation for orientationally disordered β-N_2 phase

The β-N_2 phase displays an orientationally disordered structure, so the molecules in this phase have no nominal orientation. To reach this structure from a harmonic reference, a three-part path is followed. In the first part, the temperature is increased from $T = 0$ to $T_\beta = 45$ K while the orientations of all molecules are held fixed. In the second part, the molecular rotational motions are then gradually turned on at fixed temperature, leaving the system in an orientationally disordered structure; a new targeted perturbation technique is used to compute free energies along this path. Then in the third part, the absolute free energy of the β-N_2 phase at different temperatures can conveniently be determined using the HTTP method, with scaling applied to only the molecular translational dof. To simplify our following presentation, we denote these 3 paths as *TPTrans*, *RP*, and *TP* paths, respectively. We further detail each in the following.

1. TPTrans

As the name implies, only molecular translational degrees of freedom are considered in this path. The HTTP method is employed to calculate the free energy difference for the system at different temperatures, from $T = 0.002$ K to T_β. During the simulations, the molecules are allowed to translate but their orientations are held fixed; no rotational motion is sampled. In each perturbation, the molecular displacements of the sampled system (system I) are scaled to improve the phase-space overlap with the perturbed system (system II) according to Eq. (4). Overlap sampling is used as described above.

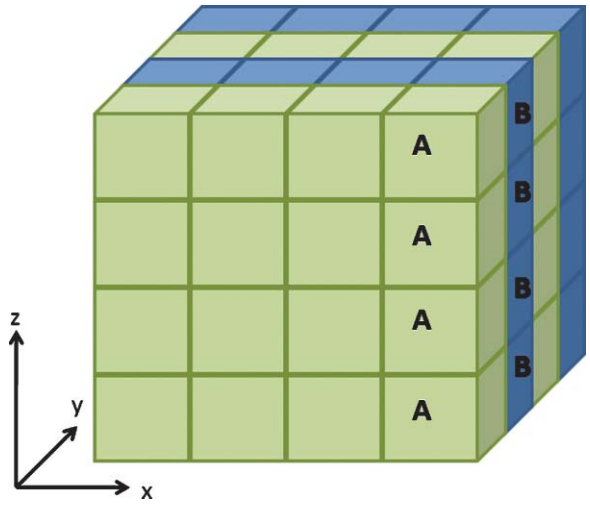

FIG. 2. Illustration of the alternating layers of unit cell A and B for the artificial "low-temperature" β-N_2 phase structure.

Referring to the nitrogen solid phase diagram,[11] the β-N_2 phase is not thermodynamically stable at low temperature. However, the HTTP method calculates the absolute free energy quantity by "connecting" the system at finite temperature to harmonic system. So, to apply the method, we must identify a mechanically stable low-temperature structure that the β-N_2 phase can connect to via a reversible path in temperature. A minimum-energy structure has to be determined by minimizing the lattice energy with respect to the molecular orientations and their lattice sites in space.

As mentioned in introduction, the β-N_2 crystal structure adopts hcp packing, which contains two basis molecules in each unit cell. Mimicking the molecular packing for the fcc α-N_2 phase, we set up two unique hcp unit cells (A and B) within which there are a total of 8 molecular rotational dof. These unit cells form A- and B-layers of cells that alternate in the y direction, which is illustrated in Fig. 2. With this construction, the number of unit cells in this direction has to be even. The search for the lowest energy structure is conducted by first placing the molecular centers of mass at the hcp basis centers, followed by screening through 4^8 configurations (considering 4 orientations for each molecule: rotating 0, $\pi/4$, $\pi/2$, and $3\pi/4$ from z axis of each). The 4-molecule basis is picked with the expectation that the "low-temperature" β-N_2 crystal structure would have a close resemblance of the low-temperature low-pressure fcc α-N_2 crystal packing.

Several lowest lattice-energy structures from the screening are then subject to lattice-energy minimization using the steepest descent method. The lattice energy of these structures is minimized not only with respect to the two dof that define molecular orientation but also the 3 translational dof as well. A total of 20 parameters (10 dof for each unit cell, A and B) are optimized. The crystal structure that gives the lowest lattice energy is selected as the low-temperature β-N_2 structure. The optimized parameters are density-specific—a new set of optimized parameters is required for each system with particular density. However, instead of going through the redundant process of global screening, we start the minimization using the parameters that are found in previous minimization at a nearby density. The parameters are first found for a 1024-particle system with density $= 0.023$ Å^{-3}. Parameters for subsequent densities, e.g., 0.0225, 0.0220, 0.0215, and 0.0210 Å^{-3} are optimized using the parameters from the next-higher density as input.

To connect *TPTrans* calculation to the harmonic system, extrapolation is applied. The harmonic system that we are treating here is the lowest-lattice energy structure that is found from the energy-minimization procedure. Rather than 5 dof for each molecule, only 3 molecular translational dof's are considered in the harmonic system. This is done to relate the harmonic reference system to the system sampled at the *TPTrans* path, where there is no molecular rotational motion. The first 9 points (0.002 K to $T_{\beta 0} = 0.020$ K with interval of 0.002) from the *TPTrans* perturbation data are fitted to a Qth-order polynomial and are extrapolated to $T = 0$ to determine $\beta A_C^{\text{fit}}/N$ that is in excess of the harmonic free energy at $T_{\beta 0}$. Then, the working equation for the free-energy calculation in this *TPTrans* path is given as

$$\frac{\beta A_{C,TPTrans}}{N}(T_\beta) = \frac{\beta A_C^{\text{fit}}}{N}(T_{\beta 0}) + \frac{1}{N}\sum_{T=T_{\beta 0}}^{T_\beta} (\Delta \beta A_C)_{T_i \to T_{i+1}} \tag{9}$$

where T_i and T_{i+1} are adjacent temperatures. The second term in the RHS of the equation is free-energy difference between systems at $T_{\beta 0}$ and T_β in the presence of coordinate scaling and the last term is the Jacobian resulting from the translational scaling.

2. RP

The rotational degrees of freedom are introduced in the second perturbation path. Here each molecule is allowed to rotate and translate in Monte Carlo (MC) fashion but with the presence of hard rotational constraint, $\theta < \theta_{\max}$, with the perturbation path tracing out increasing values of $\theta_{\max}$ (again, θ is the angle measured from the nominal orientation $\vec{a}_0$, which here is the same orientation introduced in the *TPTrans* path). At the end of the path, all molecules can rotate freely. This perturbation path utilizes a method similar to HTTP, which we call RTP, described further below.

The first step in the *RP* path is to release the molecules slightly from their fixed *TPTrans* orientations. This is accomplished by performing free-energy perturbations in which the orientations of all molecules are selected at random to deviate by small amounts from their respective nominal orientations $\vec{a}_0$. The new orientations all satisfy $\theta < \theta_{\max,1}$, where $\theta_{\max,1} = 1^\circ$ is the orientation constraint in the first step of the *RP* path. To avoid questions about free-energy singularities associated with the introduction of a new dof, we take a perspective in which this perturbation is simply coupling the molecule's orientation to its orientation coordinate, which in the non-perturbed system is uncoupled and thus free to choose any value unbiased in $\theta < \theta_{\max,1}$ (or more precisely, $\cos\theta$ is uniform in this range). The contribution to the free energy for

this dof in the uncoupled system is

$$\frac{\beta A_{\mathrm{RTP},1}}{N} = -\ln(2\pi(1-\cos\theta_{\max,1})). \tag{10}$$

The configuration space of the orientationally uncoupled system fully encompasses the configurations of the coupled system, i.e., a phase-space subset relation holds.[14] This situation makes direct perturbation effective and undemanding, so overlap sampling is not needed. The free-energy difference for this step can be conveniently expressed as

$$\frac{\beta\Delta A_{\mathrm{RTP},2}}{N} = -\frac{1}{N}\ln\left\langle\frac{e_{\mathrm{coupled}}}{e_{\mathrm{uncoupled}}}\right\rangle_{\mathrm{uncoupled}}, \tag{11}$$

where e is the Boltzmann factor of system denoted by the subscript and the angle bracket represents the canonical ensemble average that is sampled according to the Boltzmann weight of the uncoupled system.

In the next step of the *RP* path, the constraint angle, $\theta_{\max}$, is increased in a series of simulations to allow a gradual transition to the orientationally disordered phase. Perturbation is conducted along this path in increasing rotational constraint angle and the relative free energy between systems with adjacent rotational constraint angle is calculated. At constant temperature, the perturbations commence from $\theta_{\max,1}$ and eventually grow to angle of 90°, at which the molecule gains its total rotational freedom. Hence, the free energy difference of the system with small constraint angle, $\theta_{\max,1}$ and system with no rotational constraint can be determined through the described perturbation path.

Adapting the idea of harmonic scaling in the HTTP method, the free-energy perturbation calculation between two systems with different rotational constraint angles can be improved by introducing appropriate scaling to the rotational degrees of freedom. This is done with the aim to better map the phase space volumes of both systems onto each other. The scaling is most conveniently expressed in terms of the generalized coordinates introduced in Eqs. (3). Specifically, each orientation coordinate is scaled as follows:

$$\kappa_{i,II} = \kappa_{i,I}\frac{\kappa_{\max,II}}{\kappa_{\max,I}} = \kappa_{i,I}\left(\frac{1-\cos\theta_{\max,II}}{1-\cos\theta_{\max,I}}\right)^{1/2}, \tag{12}$$

where $\theta_{\max,I}$ and $\theta_{\max,II}$ are the constraint angles that distinguish systems I and II, respectively. This scaling is applied to all $2N$ orientational coordinates. Without this scaling, perturbation to larger constraint angles would be pointless, and the free-energy difference for systems having different constraint angles could be measured only in the direction toward smaller (more constraining) angles. With the scaling, perturbations in both directions can yield useful information, and overlap sampling[6] is an appropriate scheme to apply for the free-energy calculation. In this case, the ratio of partition functions of the two systems is

$$\frac{Z_{II}}{Z_I} = \frac{\langle\gamma/e_I\rangle_I}{\langle\gamma/e_{II}\rangle_{II}}\left(\frac{1-\cos\theta_{\max,II}}{1-\cos\theta_{\max,I}}\right)^N, \tag{13}$$

where the angle bracket denotes the ensemble average sampled according to sampling weight given in the subscript. We define $\exp[-\Delta\beta A_C] = \langle\gamma/e_I\rangle_{e_I}/\langle\gamma/e_{II}\rangle_{e_{II}}$. Hence, the free-energy difference between the two constraint states can be computed by using the following equation:

$$\beta(A_{II}-A_I) = (\beta\Delta A_C)_{\theta_{\max,I}\to\theta_{\max,II}} - N\ln((1-\cos\theta_{\max,II})/(1-\cos\theta_{\max,I})), \tag{14}$$

The second term at the RHS is the contribution from Jacobian. The total free energy change for transforming from the constrained system obtained at the end of the *TPTrans* path, to the unconstrained orientationally disordered system is obtained by summing the contributions from all of the constraint perturbations. The Jacobian terms largely cancel each other, except for the first term ($\theta_{\max,1}$) and the last ($\theta_{\max} = 90°$), which is zero. Further, when the first reference free energy $\beta A_{\mathrm{RTP},1}$ (Eq. (10)) is added in, it cancels the first Jacobian term as well (apart from a factor of $\ln 2\pi$). Putting it all together, the total free energy change for the *RP* path is

$$\frac{\beta A_{\mathrm{RTP}}}{N}(T_\beta) = \frac{1}{N}\sum_{i=1}(\beta\Delta A_C)_{\theta_{\max,i}\to\theta_{\max,i+1}} + \frac{\beta\Delta A_{\mathrm{RTP},2}}{N} - \ln 2\pi. \tag{15}$$

The implementation details for RTP are the same as what had been described in HTTP method.[6] For more detailed information, we kindly refer the reader to our previous work.

3. TP

Lastly, we perturb again between systems with different temperatures (*TP* path) to compute the free energy of systems with either higher or lower temperature, starting at $T = T_\beta$. The perturbation path is similar to *TPTrans* path that was described earlier using the HTTP method but with the molecular rotational motions allowed. Even though the molecules are now free to rotate, the coordinate scaling is applied only to the translational degrees of freedom since scaling the molecular rotations in the orientationally disordered phase is inappropriate.

Combining Eqs. (9) and (15), we derive the full working equation to calculate for the free energy of the β-N_2 phase:

$$\frac{\beta A}{N}(T) = \frac{\beta A_{\mathrm{harm}}}{N}(T_{\beta 0}) + \frac{\beta A_{\mathrm{RTP}}}{N}(T_\beta) + \frac{\beta A_{C,TPTrans}}{N}(T_\beta) - \frac{1}{N}\sum_{T_\beta}^{T}(\Delta\beta A_C)_{T_i\to T_{i+1}} - \frac{3}{2N}(N-1)\ln\left(\frac{T}{T_{\beta 0}}\right) \tag{16}$$

where $\beta A_{\mathrm{harm}}/N$ is given in Eq. (1) with $m = 3$.

D. Simulation details

Canonical NVT-ensemble MC simulations are conducted for all the calculations, where each system has fixed number of particles, volume, and constant temperature. No

volume-fluctuation simulations are attempted. However, several molecular densities are examined ρ [in unit Å^{-3}] ranging from 0.0230 to 0.210 in intervals of 0.001. For the fcc orientationally ordered α-N_2 phase, this crystal structure retains a cubic packing with unit cell length, a, given as $a = \sqrt[3]{4/\rho}$, where 4 is the number of basis molecules in a fcc unit cell. On the other hand, for the 2-basis molecules hcp β-N_2 phase, we adopted c/a ratio = 1.631 from the literature,[18] where c is the height of the unit cell. Both lattice parameters a and c can be determined from equations: $a = \sqrt[3]{4/(1.631 \times \sqrt{3}\rho)}$ and $c = 1.631a$ as function of density, ρ. A truncation radius of 0.475 of the simulation box length is employed. The system sizes that are examined in this study are 864 and 1024 for α- and β-N_2, respectively.

10^7 MC trial steps are sampled for each simulation. Each MC trial step consists of either a translational or a rotational move. An initial simulation of 10^6 steps is first carried out with an equilibration steps of $(1 + (N/500)) \times 100N$ where N is the number of particles in the system. To save time in equilibrating the system, each subsequent simulation initiates with the final configuration from the previous run.

In this work, the pairwise interaction between the rigid nitrogen molecules is described by the intermolecular potential model proposed by Etter *et al.*[12] This model is derived through fitting to both theoretical[19] and experimental data.[20] It has been used to study the nitrogen polymorph α-β phase transition in the past[8,9] and has proven its ability to provide a stable phase for both structures. The intermolecular potential is represented by site-site interactions, where two force centers (nitrogen atomic sites) are placed in each molecule. Atomic positions are located at ±0.547 Å from the molecular center. Electrostatic interactions are represented by placing four point charges along the molecular axis, where the positive and negative charges at ±0.847 Å and ±1.044 Å, respectively. These charges carry values of 0.373e and −0.373e. The geometry and the point-charge distribution are illustrated in Fig. 3.

The dispersion-repulsion interaction energy between atomic sites i and j in different molecules are given in Eq. (17) and the values for potential parameters in Table I. It is customary to characterize the elongation of a homonuclear dimer in terms of L^*, the ratio of the distance between the atoms divided by their characteristic diameter. If we take the diameter as the separation where the potential goes through zero (which for this model is 3.335 Å), then L^* = 0.328. The quadrupole moment of the model is 4.453 × 10^{-40} C m^2, which is slightly lower than the ideal-gas value for N_2 of about 5.0 × 10^{-40} C m^2 given by experiment and *ab initio* calculation.[21]

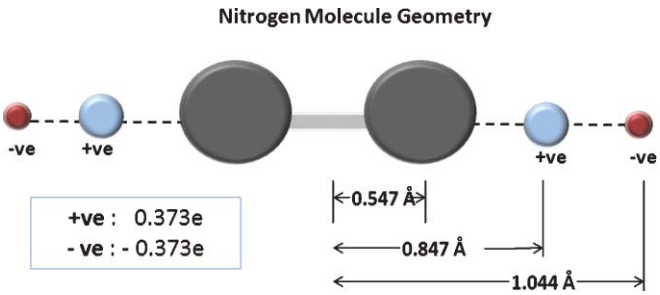

FIG. 3. Molecular geometry of Etters *et al.*'s nitrogen model. Size of nitrogen atom centers is not drawn to scale.

$$\phi(r_{ij}) = \begin{cases} A_1 \exp(-\alpha_1 r_{ij}) - B_1/r_{ij}^6, & r_{ij} \geq R_1, \quad \text{(a)} \\ \sum_{n=0}^{4} C_i (r_{ij} - R_0)^n - B_1/r_{ij}^6, & R_1 > r_{ij} \geq R_0, \quad \text{(b)} \\ A_2 \exp(-\alpha_2 r_{ij}) - B_1/r_{ij}^6, & r_{ij} < R_0. \quad \text{(c)} \end{cases} \tag{17}$$

In the course of our studies we observed a small but significant discontinuity in the potential energy for this model. It could be due to the rounding-off error introduced by Etter *et al.*'s quartic-spline-fit of the potential parameters for the intermediate separation-distance region. In order to improve the potential model, we modify the parameters C_0 and C_1 from the suggested values of 415.73107 K and −1446.74414 K Å^{-1} to 415.7168814243 K and −1446.7346714270 K Å^{-1}, respectively. This is done by adjusting C_0 and C_1 to equate the both $\phi(r_{ij})$ values calculated using Eqs. (17a) at R_1 and (17b) at R_0 to values computed using Eq. (17b) for the respective separation distance. Both reported parameters C_0 and C_1 are rounded up at the 10th decimal place.

III. RESULTS AND DISCUSSION

In much of what follows we present results from the free-energy calculations in terms the difference $\Delta(\beta A_C)$, or more precisely the quantity $\exp[-\Delta(\beta A_C)]$, which we designate as χ_i. This quantity depends on the size of the perturbation, so when plotted against the perturbation parameter it will exhibit discontinuities where the choice of the step size is changed. This anomaly could be avoided by presenting instead the free energy itself, which is the accumulation of all of the perturbation values. We choose instead to present the results in terms of χ_i because it shows our results, with their confidence limits, in a more raw form in which errors may be more easily detected.

TABLE I. Potential parameters.

$A_1/k = 9.261205 \times 10^7$ K	$C_0/k = 415.7168814243$ K	$A_2/k = 1.47248 \times 10^7$ K	$R_0 = 3.01006875$ Å
$\alpha_1 = 4.037$ Å^{-1}	$C_1/k = -1446.7346714270$ K.Å^{-1}	$\alpha_2 = 3.48$ Å^{-1}	$R_1 = 3.4494569$ Å
$B_1/k = 1.79 \times 10^5$ KÅ^6	$C_2/k = 2480.73711$ K Å^{-2}		
	$C_3/k = -2766.5419$ K Å^{-3}		
	$C_4/k = 1574.2809$ K Å^{-4}		

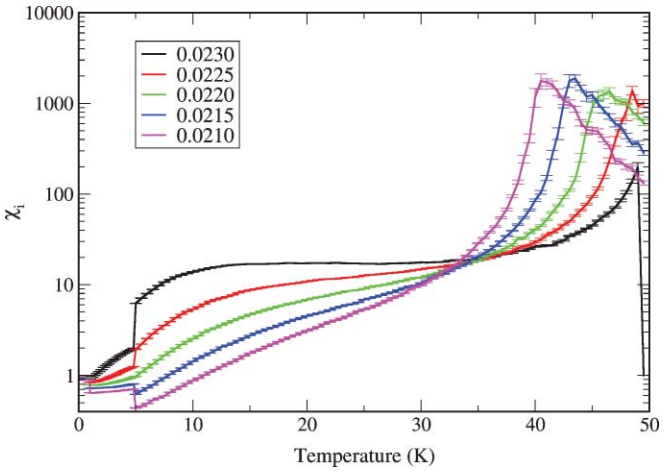

FIG. 4. χ_i vs. temperature for α-N_2. Legend indicates the molecular density in $Å^{-3}$.

A. A_C for α-N_2

In Fig. 4, we present χ_i for the α-N_2 phase at various densities, ρ [$Å^{-3}$] = 0.0230, 0.0225, 0.0220, 0.0215, and 0.0210. With constant perturbation steps in temperature, the perturbation calculation may become relatively difficult (giving larger uncertainty in χ_i) as the temperatures decreases. This is because the ratio of the phase-space volumes between the perturbing systems becomes smaller with increasing temperatures. To compensate, the perturbation steps can be made smaller so as to improve the accuracy of the perturbation results. Accordingly, several perturbation step sizes: 0.005K, 0.2K, and 0.5K are employed for this calculation, with smaller steps allocated to calculations at the low-temperature region.

As can be observed from the plot, the uncertainty for χ_i rises as the temperature increases and eventually the perturbation fails at high enough temperatures, where χ_i values are nearing the peak.

The large uncertainty in χ_i near the peak indicates that the α-N_2 phase goes through a structural transition there and becomes orientationally disordered. Further evidence for this transition is shown in Fig. 5.

Figure 5 presents the probability distribution of the system constraint, $\langle \cos\theta \rangle$ for systems of various molecular densities. At density of 0.0230 $Å^{-3}$, the $\langle \cos\theta \rangle$ distributions are sharply peaked at lower temperatures: 36, 38, 40, 42, 44, and 46 K, indicating an orientationally order phase. The distribution becomes broader as the temperature increases and eventually turns flat at 50 K. The peak in probability distribution (greater than 0.8) exhibits the order of the α-N_2 phase. However, when the molecular orientation of the system becomes equally probable (orientationally disordered), the distribution of $\langle \cos\theta \rangle$ (not shown in the figure) will peak at 0.5, wherein $\cos\theta$ is uniformly distributed from 0 to 1. The system constraint of $\langle \cos\theta \rangle > 0.8$ was intended to suppress the disorder of the system. However, as we can see from the figures, the histogram becomes nearly flat before $\langle \cos\theta \rangle$ reaches 0.8, indicating the α-N_2 phase becomes orientationally disordered before the constraint has full effect on the system. Also shown in Fig. 5, the systems start to become orientationally disordered at a lower temperature as density decreases.

B. Free-energy results and finite size effects for α-N_2

We next examine finite-size effects on the free-energy results for α-N_2 at conditions: $\rho = 0.0230$ $Å^{-3}$ and temperature

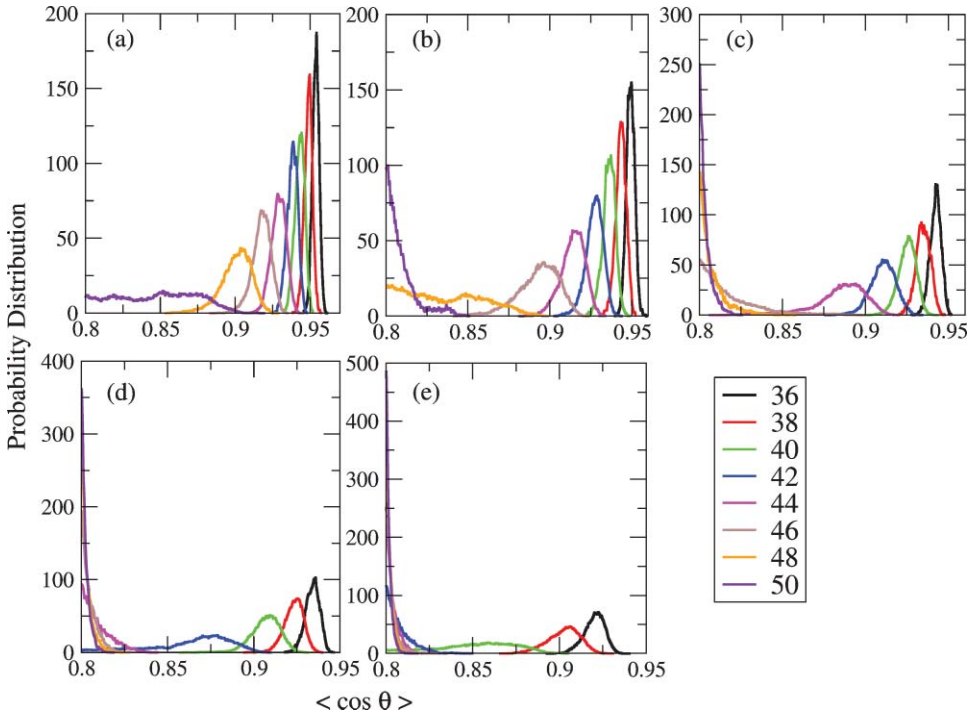

FIG. 5. Plots of $\langle \cos\theta \rangle$ probability distribution for molecular densities, ρ [$Å^{-3}$], of (a) 0.0230, (b) 0.0225, (c) 0.0220, (d) 0.0215, and (e) 0.0210. Legend indicates the temperature in Kelvin.

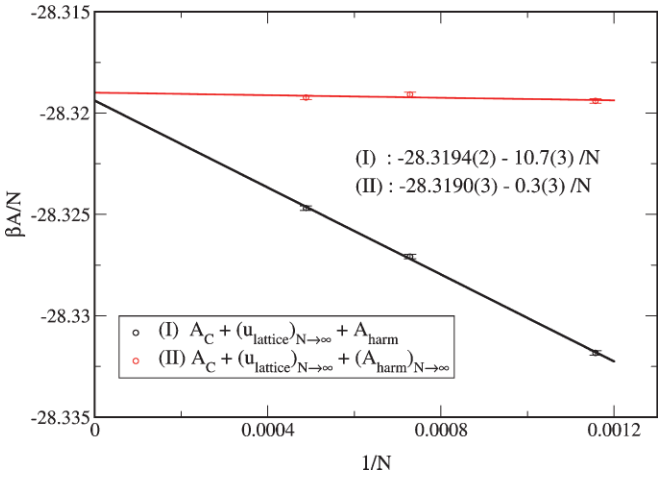

FIG. 6. Plot of $\beta A/N$ vs. $1/N$ for α-N_2 phase at $\rho = 0.0230$ Å^{-3} and $T = 30$ K, where N is the number of particles and βA/N is from Eq. (2).

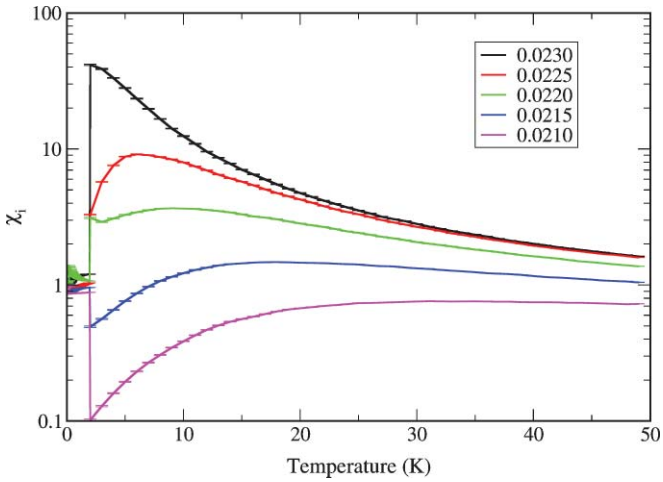

FIG. 7. *TPTrans* path. χ_i vs. temperature in Kelvin. Legend indicates molecular density in Å^{-3}.

$T = 30$ K. Figure 6 shows the Helmholtz free energy, $\beta A/N$ against $1/N$, where N is the number of molecules. The zero of the abscissa represents the infinite-sized system. In the plot, two approaches are used to obtain the free energy at the thermodynamic limit, $N \to \infty$ through extrapolation. Both approaches employ lattice energy that is calculated with a lattice sum, $(\beta U_{\text{lattice}})_{N\to\infty}$, which sums to intermolecular separations of 2.5×10^3 Å. For the first approach, the free energy is determined using the harmonic free energy, βA_{harm} and anharmonic term, βA_C, with each calculated for finite-size systems: 864, 1372, and 2046 particles. The result is then extrapolated to $1/N = 0$ to obtain the free energy for an infinite system. The second approach is the "hybridInf" method that we introduced in our previous work.[17] In this approach, the free energy is calculated by performing separate extrapolations of the harmonic and anharmonic contributions to the free energy. The infinite-system free energies found are $-28.3194(2)$ and $-28.3190(3)$ for the first and second approach respectively (indicated by (I) and (II) in Fig. 6). The last digit in the parentheses is the 67% confidence limit. Both results agree very well within each other's uncertainties. Note that the infinite-system harmonic free energy, $(\beta A_{\text{harm}})_{N\to\infty}$ given in (II) is determined through extrapolation using system sizes ranging from 2048 to 6912. As we can see from Fig. 6, the system-size dependence of the free energy (mainly from the harmonic contribution, βA_{harm}) is largely removed by using the hybrid-Inf approach, where the fitted curve gives us a statistically zero slope. The anharmonic term, βA_C, is system-size independent, consistent with what was previously found for the soft-sphere model.[6,17] The advantage offered here, of course, is that this anharmonic contribution is the only part requiring molecular simulation for its evaluation; the computational expense of the other, size-dependent contributions is mainly in performing lattice sums.

C. A_C for β-N_2

In this part of the study, we present the correction term, A_C, for the orientationally disordered β-N_2 phase, considering each perturbation path in turn. In Fig. 7, χ_i for the *TPTrans* path is presented for several densities with a system size of 1024 particles. Various perturbation intervals: 0.002 K, 0.01 K, 0.05 K, and 1.0 K are used to improve the results for systems at lower temperatures. There are only three dof considered in this path and the relative uncertainties, σ_{χ_i}/χ_i, in each perturbation for various intervals are found to be small, ranging from 0.1% to 1%.

Figure 8 presents the free-energy difference between the orientationally coupled and uncoupled systems, $\exp(-\beta\Delta A_{\text{RTP},2})$ (as given in Eq. (11)) as a function of molecular density, evaluated at $T = 45$ K. This is the first step in the *RP* perturbation path. Due to the subset relation between the orientationally coupled and uncoupled systems, the calculation through direct sampling is efficient and accurate, such that $\exp(-\beta\Delta A_{\text{RTP},2})$ has relative uncertainty that is less than 0.2%.

The variation of $\exp(-\beta\Delta A_{\text{RTP},2})$ with density in the orientationally coupled-uncoupled perturbation is consistent with the χ_i results for *RP* path (at constant temperature of 45 K) that are shown in Fig. 9. In this *RP* path, the χ_i between systems with different constraint angles, $\theta_{\max}$ decreases with

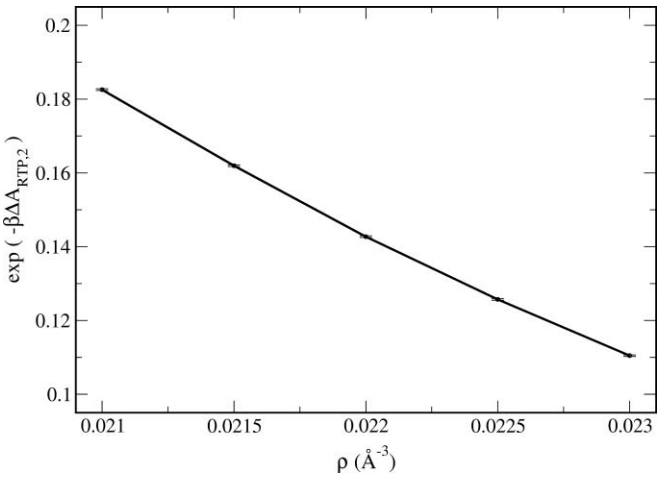

FIG. 8. Free energy difference for initial, orientation-coupling perturbation of *RP* perturbation path, as function of molecular density, ρ.

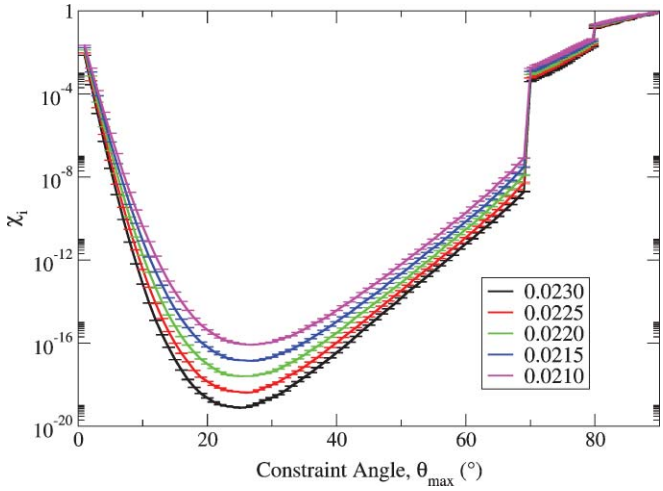

FIG. 9. *RP* path. χ_i vs. constraint angle, $\theta_{\max}$, in degrees. Legend indicates molecular density in Å^{-3}.

increasing density. The χ_i value is also observed to be consistently below unity. Various perturbation intervals are used for the *RP* path and they are 0.02°, 0.04°, and 1°. Through application of orientation-coordinate scaling to the perturbation and proper choice of perturbation interval in $\theta_{\max}$, we obtain relative uncertainty, σ_{χ_i}/χ_i of ∼2%–5%. Also observed from the Fig. 9, the χ_i value goes through a trough as the perturbation marches up in constraint angle, $\theta_{\max}$.

We next present χ_i vs. temperature for *TP* path in Fig. 10, showing data from 30 K to 50 K. We consider only the results above about 36 K, since the molecules are unable to rotate freely and adequately sample appropriate orientations at lower temperatures. The perturbations begin to fail. For all densities reported in the plot, the relative uncertainties for the perturbation results above 36 K, range approximately from 1% (for higher-temperature perturbation, $T \to 50$ K) to 4% (for lower temperature, $T \to 36$ K).

Finally, the Helmholtz free energy for the β-N_2 phase is then determined using Eq. (16) with the anharmonic term, βA_C, calculated by combining the results from these different perturbation paths.

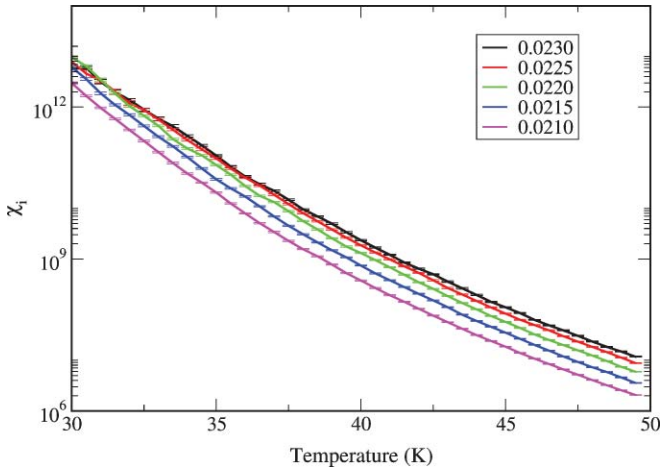

FIG. 10. *TP* path.χ_i vs. temperature in Kelvin. Legend indicates molecular density in Å^{-3}.

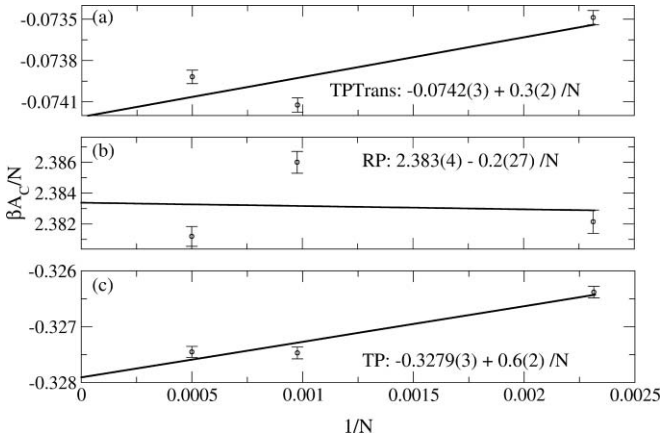

FIG. 11. $\beta A_C/N$ vs. $1/N$ plot for different perturbation paths at $\rho = 0.0230$ Å^{-3} with 432-, 1024-, and 2000-particle system sizes. The perturbation paths presented in the plot are (a) *TPTrans*, (b) *RP*, and (c) *TP*.

D. Finite size effects for β-N_2

We next examine the finite size effect for the anharmonic terms, βA_C, calculated in each perturbation path: *TPTrans*, $(\frac{1}{N}\sum_{T_i=T_{\beta 0}}^{45}(\Delta\beta A_C)_{T_i\to T_{i+1}})$, *RP* $(\frac{1}{N}\sum_{i=1}^{90}(\beta\Delta A_C)_{\theta_{\max,i}\to\theta_{\max,i+1}})$, and *TP* $(\frac{1}{N}\sum_{T_i=45}^{50}(\Delta\beta A_C)_{T_i\to T_{i+1}})$ at density of 0.0230 Å^{-3} with 432-, 1024-, and 2000-particle system sizes. As we can observe from Figs. 11, the anharmonic-term results do not scale linearly with $1/N$ and the fitted line lies outside the 67% confidence (σ) of the data points. The extrapolated free energies for the infinite-sized system have uncertainties that are approximately three times (3σ) as large, compared to the uncertainties of the fitted data. The uncertainties in the fitted coefficients are mainly due to the lack of linearity in the data points. Note that all the data presented are obtained from averaging 100 data sets from a single 10-million MC-steps simulation. As a check on the uncertainty in each calculation, we ran 5 additional independent simulations, each with 2 million MC steps, and then calculated the average values with standard error from the 5 independent samples collected. We found that the uncertainties in these results are consistent with the uncertainties from the initial calculation, as are their average values.

The lack of linearity in the anharmonic term makes it difficult to establish a precise value of the free energy in the thermodynamic limit. Nevertheless we can still see that the variations with system size are relatively small. Though the deviations from linearity may look prominent in the expanded plots, in terms of contributions to the free energy, the variations (based on βA_C of RP) with system size are less than 0.05% of the contribution of the lattice energy. Even in comparison to the harmonic contribution, the variation is small. This is demonstrated in Fig. 12, where we present the total reduced Helmholtz free energy at $T = 45$ K as a function of reciprocal of system size, N. The two approaches demonstrated in Sec. III B are employed to further study the finite-size effects for the β-N_2 free-energy calculation. The slope of the fitted curve from the hybridInf approach is statistically zero. In contrast, the calculation from approach (I) gives a slope of

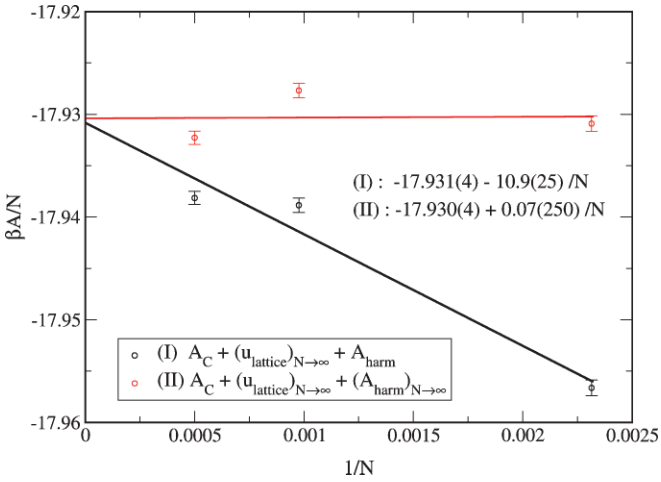

FIG. 12. Plot of $\beta A/N$ vs. $1/N$ for β-N_2 phase at $\rho = 0.0230$ Å^{-3} and $T = 45$ K, where $\beta A/N$ is from Eq. (16). The harmonic contribution represents that formulated at the outset of the *TPtrans* path, and thus is defined with respect to the system with rigid molecular orientations.

10.9. The slopes show that again the anharmonic term, βA_C, is less dependent on the system size as compared to the harmonic contribution.

E. Examination of contributing terms in Helmholtz free energy

In this section, we examine the contributing terms in the Helmholtz free-energy calculation as defined in Eq. (2). The Helmholtz free energies, A, for both α-N_2 and β-N_2 are computed using Eqs. (4) and (16) for densities [Å^{-3}] ranging from 0.0210 and 0.0230 with density interval of 0.001, over a range of temperatures where each phase is stable. The largest uncertainties for the Helmholtz free energies per particle, A/Nk, that we calculated for the α-N_2 and β-N_2 phases are ~0.01 K and 0.04 K, respectively. Note that the hybridInf approach briefly described in Sec. III B is employed for the Helmholtz free-energy calculation throughout this work.

Referring to Eq. (2), the full free-energy calculation involves computation of (a) the lattice energy, (b) the harmonic free energy, and (c) the anharmonic term, A_C. Both lattice-energy and harmonic-free-energy calculations are analytic and have no uncertainty, so the only term that contributes to the uncertainty of the free-energy result comes from the anharmonic, A_C calculation. In Table II, we illustrate and break down the Helmholtz free-energy calculation for the α-N_2 phase at $\rho = 0.0230$ Å^{-3} and $T = 49$ K. The lattice energy, harmonic free energy and anharmonic contribution at this condition are calculated in unit Kelvin to be −1031.4480141659, 244.9801604528, and −15.28(1), respectively. Both the lattice energy and harmonic free energy are of comparable orders of magnitude while the anharmonic term is ~1.5% of the value of the lattice energy.

Even though the anharmonic term, A_C term is small when compared to the lattice energy or harmonic free energy, its significance can be crucial in characterizing relative stability of crystalline phases, especially when the free-energy difference of both phases is small. As demonstrated in Table II, at $\rho = 0.0230$ Å^{-3} and $T = 49$ K, the free-energy calculation for the α-N_2 phase changes quite significantly when additional terms, for instance the harmonic free energy, A_{harm}, and anharmonic, A_C, term, are added to the lattice energy. As a result (although it may not be a direct representation in Table II), depending on which contributing terms are included in the free-energy calculation, the inclusion of different contributing terms may affect the outcome of the crystal-structure prediction results.

Also in the Table II, we report the lattice energy (given by the minimum-energy structure that we optimized in Sec. II C) and the free energy for the structure corresponding to the orientationally disordered β-N_2 phase. Comparisons are made between the α-N_2 and β-N_2 phase to determine their relative stabilities by considering different contributions to the Helmholtz free-energy calculation. Considering the lattice energy alone would indicate that the α-N_2 phase is more stable than the β-N_2; however, the full free-energy calculation (inclusive of the harmonic and anharmonic contributions) favors the β-N_2 phase at $\rho = 0.0230$ Å^{-3} and $T = 49$ K. We next considered including the harmonic contribution to both phases. Although we previously performed 3-dof (translation only) harmonic analysis for the β-N_2 phase, we have repeated the analysis including rotation (5 dof) for the value reported in Table II. We found that the harmonic α-N_2 structure is more stable than the β-N_2 structure (with rotational dof) and the inclusion of the harmonic contribution yields difference in stability between the two phases that is slightly smaller than the calculation done merely using the lattice energy. The point of this exercise is to demonstrate the importance of all contributions to the free-energy calculation, particularly when used (as is often the case) to examine small differences in stability of competing phases.

F. Relative stability of α-N_2 and β-N_2 phases

Next, we examine the relative stability between the α-N_2 and β-N_2 phase based on their Gibbs free energies, $G(P, T)$. The pressure and energy of the systems are determined through the derivatives of the Helmholtz free energy with respect to density, ρ, and inverse temperature, β, respectively, which are shown in the equations below:

$$P = \rho^2 \left(\frac{\partial A}{\partial \rho} \right), \tag{18a}$$

$$U = \frac{\partial \beta A}{\partial \beta}. \tag{18b}$$

At the occurrence of a phase transition, the temperature, pressure, and chemical potential (Gibbs free energy) of both phases are identical. In Fig. 13, we plot Gibbs free energy per particle as a function of temperature at constant pressure. The pressures examined in the plot are 0.0, 0.1, 1.0, 2.0, 5.0, and 10.0 MPa. From the plot, we determine the transition temperatures at each respective pressures, where both lines cross, indicating $\Delta G = 0$. The transition properties, such as the coexistence densities, for the α-N_2 and β-N_2 phase are also computed.

TABLE II. Examination of contributing terms in Helmholtz free-energy calculation per particle [in unit Kelvin] for α-N_2 and β-N_2 phase at $\rho = 0.0230$ Å^{-3}, and $T = 49$ K. The last digit in the parentheses is the 67% confidence limit.

Contribution terms	α-N_2	β-N_2	$\alpha - \beta$
U_{lat}/N	−1031.4480141659	−997.1448294779	−34.3031846880
$U_{lat}/N + A_{harm}/N$	−786.4678537131	−765.8202944100[a]	−20.6475593031
$U_{lat}/N + A_{harm}/N + A_C/N$	−801.75(1)	−802.26(4)	+0.51(4)

[a]Harmonic free energy for β-N_2 phase that is computed with 5 dof.

At atmospheric pressure (0.1 MPa), we have found that the α-N_2 phase undergoes solid-solid phase transition into β-N_2 phase at temperature of 40.35(1) K. The coexistence densities are 0.021490(1) Å^{-3} and 0.021154(9) Å^{-3} for the α-N_2 and β-N_2 phase, respectively. The volume change and entropy difference between the two phases at phase coexistence for $P = 0.1$ MPa are also determined and they are 0.44(1) cm^3/mol and 1.99(1) cal/mol · K. The reported stochastic uncertainty for this transition-property study is gauged by generating random values of all uncertain χ_i values of the α-N_2 and β-N_2 phases, sampling each from a Gaussian of mean and standard deviation consistent with the value and standard error of the respective value. Each set of perturbed values is used to determine a new set of transition properties, and these values are then subject to standard error analysis. A similar calculation to determine the α-β phase transition was carried out by Kuchta *et al.*[9] Even though the transition temperature (at $P = 0.1$ MPa) that we found is close to the one obtained in their work, which is 41.0(8) K, we are not able to make comparisons between the two results. This is due to the fact that in this previous work,[9] Helmholtz free energy was used to locate the α-β phase transition and also important details of their calculations, e.g., system size, density, and pressure, were omitted.

In order to verify the transition-property results that we have found, we apply the Clapeyron relation, $dP/dT = \Delta S/\Delta V$, as a check of consistency. The coexistence curve for α-N_2 and β-N_2 phase on a P-T diagram is traced from zero pressure up to 0.12 GPa, See Fig. 14. The slope of the P-T curve given in the LHS of the Clapeyron equation is compared with the ratio of calculated entropy, ΔS, and volume change, ΔV, from the RHS of the equation. Both quantities that are determined separately from the RHS and LHS of the relation agree well with one another (not shown), validating the coexistence points that were computed in this work.

In Fig. 14, we present the coexistence curve for α-N_2 and β-N_2 phase that is found through this work along with the one determined experimentally from the literature.[22] The slopes of both curves are fairly consistent with each other. However, we observe that there is a shift of ∼5 K in the curve calculated in this work compared to the experiment. This discrepancy can be due to the inadequacy of the potential model in describing the phase transition of the α-N_2 and β-N_2 phase. We want to emphasize that our work is primarily geared toward testing the free-energy calculation technique that we develop and improvement of the potential model (apart from addressing the anomalies described in Sec. II D) is outside the scope of this current study. Nevertheless, through the techniques we develop in this work, we are able not only to calculate the free energies for both the orientationally ordered α-N_2 and plastic β-N_2 phase with high precision but also to characterize the α-β coexistence curve from 0 to 0.12 GPa (as shown in Fig. 14). We mention in passing that we performed lattice-enthalpy calculations to examine the stability of the α-N_2 and β-N_2 phase with varying pressures. We find that the lattice enthalpy predicts the α-N_2 phase to be more stable than the β-N_2 phase at all conditions of pressure (neglect of entropic contributions

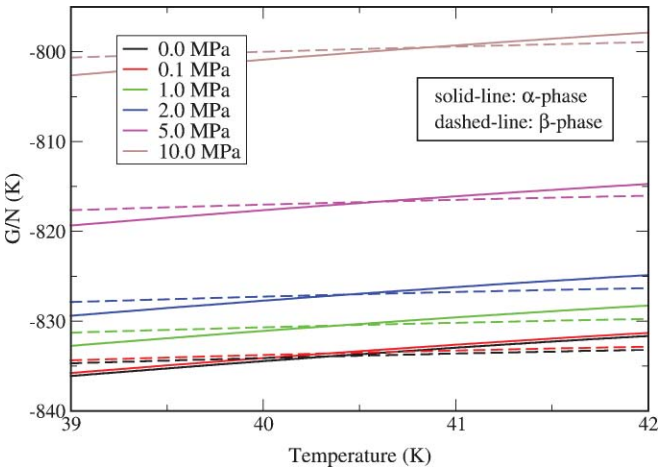

FIG. 13. Plot of Gibbs free energy vs. temperature. Legend indicates the pressure for each set of curves.

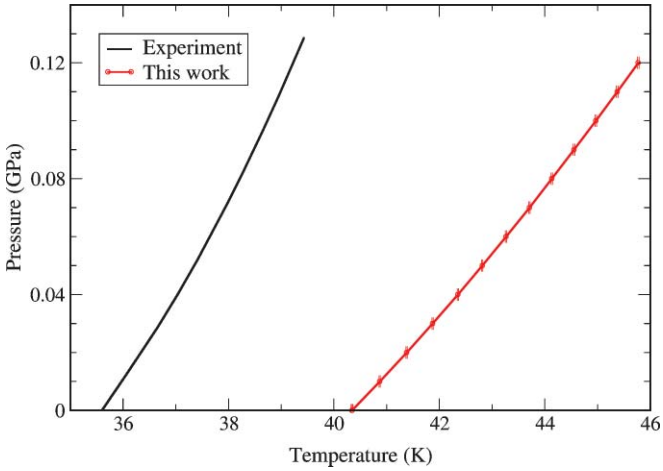

FIG. 14. P-T diagram of solid-phase nitrogen. α-N_2 is stable at lower temperatures and β-N_2 is at higher temperatures. The uncertainty reported for the data from this work is about the size of the symbols.

means that no temperature effects can be considered in such an analysis).

IV. CONCLUSIONS

We have presented novel techniques to calculate the absolute free energy for both the orientationally ordered and disordered nitrogen molecular model. These techniques are extensions of the HTTP method that utilizes the Bennett-optimized overlap sampling with targeted perturbation to determine the anharmonic term, A_C (in excess of harmonic free energy). In these techniques, the absolute free energy of the molecular system is calculated through combination of the lattice energy and harmonic free energy with the anharmonic term. The free-energy calculation results from these techniques have shown to be highly precise. This is mainly attributed to (a) the high-precision calculation results in the A_C and also (b) the calculations of lattice energy and harmonic free energy that are truly analytic and uncertainty free.

In this work, we have again demonstrated that the anharmonic term, A_C, has weak dependence on system size, suggesting that this finding applies not only to monatomic atomistic models, e.g., soft-sphere model[6,17] but also to multiatomic molecular models as well. The weak system-size dependency of the anharmonic contribution as observed here reinforces our previous suggestion that the absolute free energy of a target system in the thermodynamic limit can be estimated most efficiently by calculating the lattice energy and harmonic free energy for a large (infinite-size limit) system and then correcting the free energy with A_C using simulation methods applied to small systems. And lastly, we have succeeded in calculating the α-β transition properties and tracing the coexistence curve from zero pressure up to 0.12 GPa with the free-energy results obtained from these techniques.

ACKNOWLEDGMENTS

Acknowledgment is made to the Donors of the American Chemical Society Petroleum Research Fund for partial support of this research. Additional support has been provided by the U.S. National Science Foundation, Grant No. CHE-0626305. Computational resources were provided by the University at Buffalo Center for Computational Research.

[1]S. R. Chemburkar, J. Bauer, K. Deming, H. Spiwek, K. Patel, J. Morris, R. Henry, S. Spanton, W. Dziki, W. Porter, J. Quick, P. Bauer, J. Donaubauer, B. A. Narayanan, M. Soldani, D. Riley, and K. McFarland, Org. Process Res. Dev. **4**(5), 413 (2000).
[2]G. M. Day, T. G. Cooper, A. J. Cruz-Cabeza, K. E. Hejczyk, H. L. Ammon, S. X. M. Boerrigter, J. S. Tan, R. G. Della Valle, E. Venuti, J. Jose, S. R. Gadre, G. R. Desiraju, T. S. Thakur, B. P. van Eijck, J. C. Facelli, V. E. Bazterra, M. B. Ferraro, D. W. M. Hofmann, M. A. Neumann, F. J. J. Leusen, J. Kendrick, S. L. Price, A. J. Misquitta, P. G. Karamertzanis, G. W. A. Welch, H. A. Scheraga, Y. A. Arnautova, M. U. Schmidt, J. van de Streek, A. K. Wolf, and B. Schweizer, Acta Crystallogr. **65**, 107 (2009); G. M. Day, W. D. S. Motherwell, H. L. Ammon, S. X. M. Boerrigter, R. G. Della Valle, E. Venuti, A. Dzyabchenko, J. D. Dunitz, B. Schweizer, B. P. van Eijck, P. Erk, J. C. Facelli, V. E. Bazterra, M. B. Ferraro, D. W. M. Hofmann, F. J. J. Leusen, C. Liang, C. C. Pantelides, P. G. Karamertzanis, S. L. Price, T. C. Lewis, H. Nowell, A. Torrisi, H. A. Scheraga, Y. A. Arnautova, M. U. Schmidt, and P. Verwer, *ibid.* **61**, 511 (2005); J. P. M. Lommerse, W. D. S. Motherwell, H. L. Ammon, J. D. Dunitz, A. Gavezzotti, D. W. M. Hofmann, F. J. J. Leusen, W. T. M. Mooij, S. L. Price, B. Schweizer, M. U. Schmidt, B. P. van Eijck, P. Verwer, and D. E. Williams, *ibid.* **58**, 647 (2002).
[3]A. Gavezzotti and G. Filippini, J. Am. Chem. Soc. **117**(49), 12299 (1995).
[4]P. A. Monson and D. A. Kofke, Adv. Chem. Phys. **115**, 113 (2000).
[5]D. Frenkel and A. J. C. Ladd, J. Chem. Phys. **81**(7), 3188 (1984); J. M. Polson, E. Trizac, S. Pronk, and D. Frenkel, *ibid.* **112**(12), 5339 (2000).
[6]T. B. Tan, A. J. Schultz, and D. A. Kofke, J. Chem. Phys. **133**(13), 134104 (2010).
[7]A. F. Schuch and R. L. Mills, J. Chem. Phys. **52**(12), 6000 (1970).
[8]B. Kuchta, K. Rohleder, R. D. Etters, and J. Belak, J. Chem. Phys. **102**(8), 3349 (1995).
[9]B. Kuchta, K. Rohlender, D. Swanson, and R. D. Etters, J. Chem. Phys. **106**(16), 6771 (1997).
[10]A. Mulder, J. P. J. Michels, and J. A. Schouten, J. Chem. Phys. **105**(8), 3235 (1996); M. B. Sweatman, A. Atamas, and J. M. Leyssale, *ibid.* **130**(2) (2009); C. Vega, B. Garzon, S. Lago, and P. A. Monson, J. Mol. Liq. **76**(3), 157 (1998); C. Vega and P. A. Monson, J. Chem. Phys. **102**(3), 1361 (1995).
[11]R. L. Mills, B. Olinger, and D. T. Cromer, J. Chem. Phys. **84**(5), 2837 (1986).
[12]R. D. Etters, V. Chandrasekharan, E. Uzan, and K. Kobashi, Phys. Rev. B **33**(12), 8615 (1986).
[13]C. Jarzynski, Phys. Rev. E **65**(4), 046122 (2002).
[14]D. Wu and D. A. Kofke, J. Chem. Phys. **123**(5), 054103 (2005).
[15]C. H. Bennett, J. Comput. Phys. **22**(2), 245 (1976).
[16]M. T. Dove, *Introduction to Lattice Dynamics* (Cambridge University Press, New York, 2005).
[17]T. B. Tan, A. J. Schultz, and D. A. Kofke, J. Chem. Phys. **132**(21), 214103 (2010).
[18]B. M. Powell, G. Dolling, and H. F. Nieman, J. Chem. Phys. **79**(2), 982 (1983).
[19]R. M. Berns and A. Vanderavoird, J. Chem. Phys. **72**(11), 6107 (1980).
[20]R. Lesar and R. G. Gordon, J. Chem. Phys. **78**(8), 4991 (1983).
[21]A. Halkier, S. Coriani, and P. Jorgensen, Chem. Phys. Lett. **294**(4–5), 292 (1998).
[22]C. A. Swenson, J. Chem. Phys. **23**(10), 1963 (1955).